PAPER

Check for updates

Ag$_2$S quantum dots *in situ* coupled to hexagonal SnS$_2$ with enhanced photocatalytic activity for MO and Cr(vi) removal†

Jie Liu,[a] Liquan Jing,[a] Guofang Gao,[a] Yuanguo Xu, [iD] *[a] Meng Xie,[b] Liying Huang,[a] HaiYan Ji,[a] Jimin Xie [iD] *[a] and Huaming Li [iD][a]

A novel visible-light-driven Ag$_2$S/SnS$_2$ composite photocatalyst was successfully fabricated *via* a simple *in situ* hydrothermal-ion-exchange method. The materials were systematically characterized by various techniques. XRD, XPS, and TEM analysis demonstrated the successful formation of Ag$_2$S quantum dots on the surface of SnS$_2$ nanoplates. The Ag$_2$S/SnS$_2$ composite materials exhibited increased photocatalytic activity compared to pure SnS$_2$ for the removal of methyl orange (MO) and Cr(vi), and the 1% Ag$_2$S/SnS$_2$ composite material showed the best activity under visible light irradiation. Holes (h$^+$) and superoxide radicals ($^{\bullet}$O$_2{}^-$) were the major active species during the photocatalytic process. The *in situ* formation of Ag$_2$S quantum dots provided an effective way to facilitate carrier transfer and separation, which is believed to be responsible for the enhanced photocatalytic performance.

1. Introduction

Nowadays, environmental pollution and energy issues have hindered the sustainable development of modern society. Among them, the excessive discharge of industrial wastewater containing both organic pollutants and heavy metal irons at the same time is a major problem. Worse still, both organic pollutants such as methyl orange (MO) and heavy metal ions like Cr(vi) produce serious harm to the environment.[1,2] Therefore, how to remove these two types of pollutant efficiently and economically becomes an urgent issue. Semiconductor photocatalysis, as an efficient and promising technology directly utilizing solar energy to solve the environmental pollution and energy demand problems, has aroused considerable attention in the past decades.[3,4] Hitherto, various kinds of semiconductor materials (such as TiO$_2$,[5] Fe$_2$O$_3$,[6] AgVO$_3$,[7] CdS[8]) have been developed for the photodegradation of organic pollutants or the photoreduction of heavy metal ions. However, some semiconductors like TiO$_2$ only can be excited under UV light irradiation due to its wide band gap ($\sim$3.2 eV), which restricts its practical applications.[5,9] Therefore, to explore visible-light response and high-performance photocatalysts is a key objective for researchers.

Among a large variety of semiconductor photocatalysts, tin disulfide (SnS$_2$), a peculiar CdI$_2$-structure metal-sulfide

semiconductor, depend on its excellent oxidation resistance, splendid thermal stability in the air and non-toxicity, low cost,[10–15] has been in-depth investigated and widely applied in the photocatalysis field involving reduction of CO$_2$,[16] reduction of Cr(vi),[17] degradation of organic compounds,[18] and production of H$_2$ from water.[19] As the research goes on, different morphologies of SnS$_2$ nanomaterials have been obtained (such as nanoflowers,[20] nanotubes,[21] nanorods,[22] and nanoplates[23]) to produce higher specific area or control the band gap energies. Even so, the photocatalytic ability of SnS$_2$ still has been limited by the high recombination rate of photo-generated carriers.[24] Numerous strategies have been carried out to overcome this limitation, particularly, constructing suitable semiconductor composites is a powerful and effective method and various different composites with oxides (SnO$_2$,[25] Al$_2$O$_3$,[26] TiO$_2$[27]), sulfides (CdS,[28] SnS$_2$,[29] In$_2$S$_3$[30]), and others (ZnFe$_2$O$_4$,[31] g-C$_3$N$_4$,[32] rGO[33]), have been successful synthesized.

Recent years, silver sulfide (Ag$_2$S), as a direct semiconductor material with narrow band gap, possesses a high absorption coefficient and excellent conductivity properties, attracts substantial research interest and has been widely applied in sustainable photocatalysis field.[34–36] Up to now, a series of researches have been employed to use nanosized Ag$_2$S or Ag$_2$S quantum dots to modify some materials in order to obtain higher photocatalytic properties such as Ag$_2$S–SnO$_2$,[37] ZnS–Ag$_2$S,[38,39] Ag$_2$S/TiO$_2$,[40] CuS/Ag$_2$S[41] and so on. However, according to our knowledge, there is still no research compositing Ag$_2$S quantum dot with hexagonal SnS$_2$ to minimize the recombination rate of photo-generated carriers and further promote the photocatalytic property of SnS$_2$. Therefore, it is highly desirable

[a]School of Chemistry and Chemical Engineering, Institute for Energy Research, Jiangsu University, Zhenjiang 212013, P. R. China. E-mail: xuyg@ujs.edu.cn; xiejm391@sohu.com

[b]School of Pharmacy, Jiangsu University, Zhenjiang 212013, P. R. China

† Electronic supplementary information (ESI) available. See DOI: 10.1039/c7ra08369f

to synthesis Ag_2S/SnS_2 composite materials for removing the organic pollutants and heavy metal ions efficiently.

Inspired by the above ideas, in this study, a new type of Ag_2S/SnS_2 composite photocatalysts was synthesized *via* a simple *in situ* strategy, and determined by XRD, XPS, TEM, DRS, and some other techniques in detail. The experimental results showed that, Ag_2S/SnS_2 composite can achieve significantly enhanced photocatalytic performance for the removal of MO and $Cr(VI)$, indicating that the excellent electron conductivity property of Ag_2S can be used sufficiently. The reusability of Ag_2S/SnS_2 composite was examined. Finally, combining with the ESR and active species trapping results, a possible photocatalytic mechanism for the enhanced photocatalytic performance was presented.

2. Experimental

2.1 Materials

All chemical reagents and solvents were of analytical reagent grade and used as received.

2.2 Catalysts synthesis

Synthesis of SnS_2 nanoplates. The SnS_2 nanoplates were designed by a facile hydrothermal method. Specific steps are as follows: first of all, 2.1 g of tin tetrachloride pentahydrate ($SnCl_4 \cdot 5H_2O$), 3 g of thiourea and 60 mL of deionized water were mixed with ultrasonic for 10 min, then transferred into a 100 mL Teflon-lined autoclave and heated at 180 °C for 12 h. The yellow precipitates were centrifuged and washed several times, then dried at 60 °C for 12 h in vacuum.

Synthesis of Ag_2S/SnS_2 composite materials. The formation of Ag_2S/SnS_2 composite materials was described as the following steps: firstly, 0.1 g of SnS_2 nanoplates were dispersed in 40 mL of deionized water, followed by ultrasonic and stirring for 20 min and 30 min, respectively, then added a certain amount of $AgNO_3$ (0.1 mol L^{-1}) by dropping with stirring for another 2 h. The solubility products (Ksp) of SnS_2 (2×10^{-27}) is less than that of Ag_2S (6.3×10^{-50}). Through the cation–exchange reaction between SnS_2 and Ag^+, Ag_2S is deposited preferentially on the surface of the SnS_2 nanoplates by *in situ* reaction. Then the products were washed with deionized water and absolute ethanol for several times, then dried at 60 °C for 12 h in air. Finally, the Ag_2S/SnS_2 composites were obtained. By adding different volume percentage of $AgNO_3$ to control the quality of the compound of Ag_2S, resulting in 0.5% Ag_2S/SnS_2, 1% Ag_2S/SnS_2, 3% Ag_2S/SnS_2, 5% Ag_2S/SnS_2 composite photocatalytic materials. The inductively coupled plasma atomic emission spectroscopy (ICP) analysis was investigated to determine the values of Ag^+ and Sn^{4+} concentration (Fig. S1†), then we calculated the molar ration of elements for all samples in details according to the analysis of ICP and the result are shown in Table S2.† The schematic of the preparation process is shown in Scheme 1.

2.3 Characterization

The crystal structure of samples was determined by a Shimadzu XRD-6000 X-ray diffractometer (Cu Kα radiation). Transmission
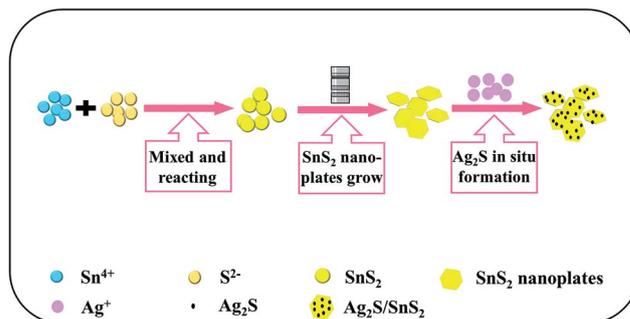
Scheme 1 Schematic of the preparation process.

electron microscopy (TEM, JEOL JEM 2010, 200 kV) were used to observe the morphologies and structures of Ag_2S/SnS_2 composites. Energy dispersive X-ray spectroscope (EDS) was used to analyze the elementary composition. X-ray photoelectron spectroscopy (XPS, VG-MultiLab 2000 system, Mg Kα) was applied to the surface analysis of samples. The optical properties of samples were analyzed by a UV-2450 Shimadzu UV-vis spectrophotometer, where $BaSO_4$ powder played the role of internal reflectance standard. The photoluminescence (PL) spectra of the as-prepared samples were investigated on a Varian Cary Eclipse Fluorescence spectrometer with an excitation wavelength of 360 nm. To investigate the transfer rate of the photo-induced carriers for the as-prepared samples, the electrochemical impedance spectroscopy (EIS) were performed in an electrochemical workstation, in which Ag/AgCl and a platinum wire and were used as reference and counter electrode, respectively. Meanwhile, the working electrode was photocatalyst (0.1 mg) films coated on ITO (0.5×1 cm^2). The ESR spectra were taken on an ESR spectrometer (JES-FA200) with DMPO (Sigma Chemical Co.) as the spin-trap reagent dispersed in water and methanol, respectively.

2.4 Photocatalytic activity

The photocatalytic activities of the SnS_2 and Ag_2S/SnS_2 composites were performed by the degradation of MO and

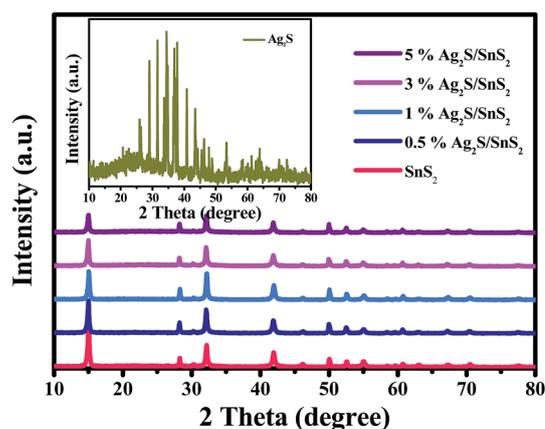**Fig. 1** XRD patterns of pure SnS_2 and Ag_2S/SnS_2 composites with different Ag_2S contents (0.5%; 1%; 3%; 5%). Inset: XRD patterns of pure Ag_2S.
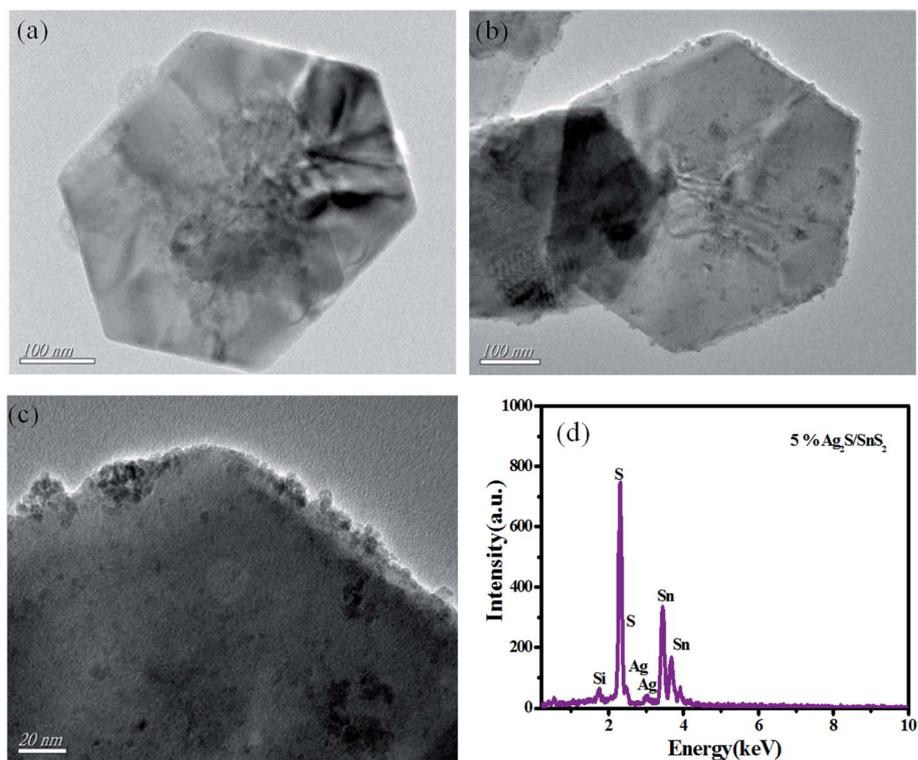
Fig. 2 TEM images of (a) SnS_2; (b and c) 1% Ag_2S/SnS_2 composite; (d) EDS analysis of 5% Ag_2S/SnS_2 composite sample.

reduction of Cr(VI) irradiated by a 300 W Xe lamp with a 420 nm cutoff filter. The photocatalytic experiment was taken with a circulating water system controlling the temperature in 30 °C

to avoid the thermal catalytic effects. Specific experimental details are as follows, 70 mg as-prepared samples were totally dispersed in 70 mL MO (10 mg L^{-1}) and $K_2Cr_2O_7$ (50 mg L^{-1})
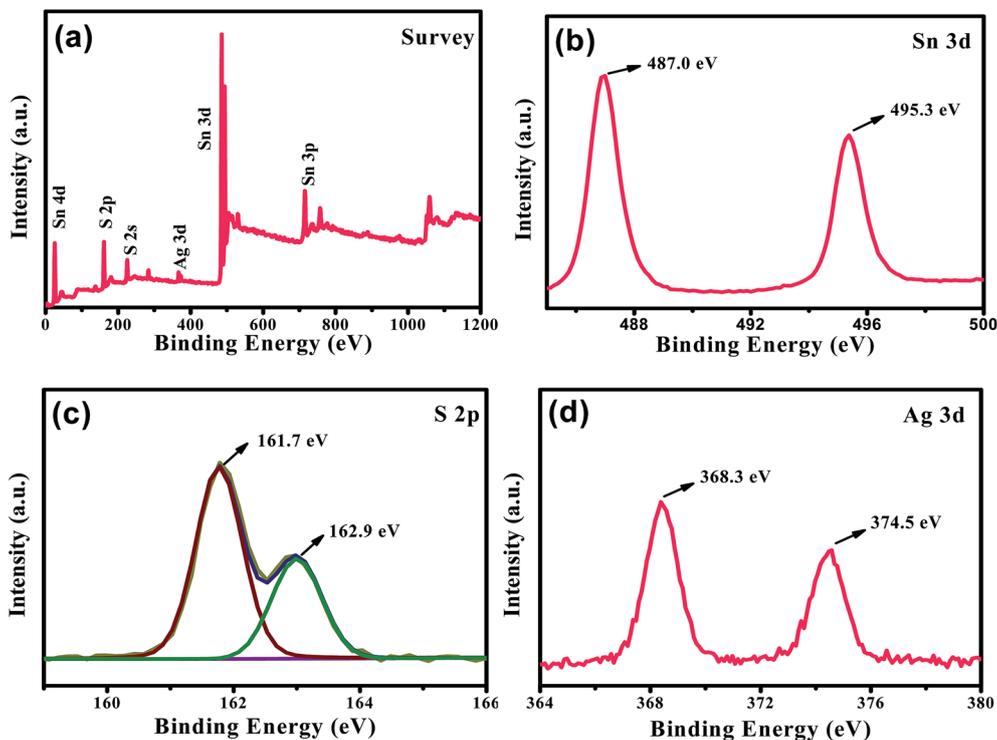

Fig. 3 XPS spectra of 1% Ag_2S/SnS_2 sample: (a) full spectra; (b) Sn 3d; (c) S 2p; (d) Ag 3d.

aqueous solution, respectively, and then the mixed solution was magnetically stirred for 30 min in the dark to obtain the absorption–desorption equilibrium, after which the reaction solution was irradiated for 60 min and about 4 mL solution was taken out in each 10 min and centrifuged. The concentrations of MO were determined on a UV-vis spectrophotometer (Shimadzu, UV-2450). The concentrations of Cr(VI) were analyzed by the following steps: 1 mL of the supernatant and 9 mL of sulfuric acid solution (0.2 mol L^{-1}) diluted in the volumetric flask, then added 0.2 mL of chromogenic agent (0.25% DPC dissolved in acetone) followed by shaking and putting it aside for 15 min, to ensure complete coloration. Finally, the absorbance was measured at a wavelength of 540 nm using a UV-vis spectrophotometer.

3. Results and discussion

3.1 Characterization of samples

The crystal structures of Ag_2S, SnS_2 and Ag_2S/SnS_2 composite materials with different Ag_2S contents were investigated by XRD analysis, as shown in Fig. 1. The diffraction peaks of pure SnS_2 can well be indexed to hexagonal SnS_2 (JCPDS 23-0677) with $2\theta = 15.03°$, $28.20°$, $32.12°$, $41.89°$ and $49.96°$, which are consistent with (001), (100), (101), (102) and (110) diffraction planes.[42] The diffraction peaks of pure Ag_2S are indexed to the standard card of pure monoclinic Ag_2S (JCPDS 14-0072).[38] For Ag_2S/SnS_2 composite materials, no Ag_2S phase can be observed, which may be due to the low amount of Ag_2S, and no obvious change is observed compared to pure SnS_2, indicating that the introduction of Ag_2S doesn't affect the crystal structure of SnS_2.

The microscopic morphologies and surface microstructures of the Ag_2S/SnS_2 composite materials were determined by the transmission electron microscopy (TEM). The pure SnS_2 nanoplate (Fig. 2a) presents a smooth hexagonal structure with a diameter of about 400 nm, which has a large surface area for the *in situ* formation of Ag_2S. The morphology of 1% Ag_2S/SnS_2 composite material (Fig. 2b) is similar to pure SnS_2, which can be further seen in Fig. 2c, the Ag_2S quantum dots have intimately attached on the surface of SnS_2 nanoplates.[43] The EDS analysis (Fig. 2d) of Ag_2S/SnS_2 composite samples displayed only Ag, Si, S and Sn elements with no other elements, indicating that Ag_2S/SnS_2 composite materials were successfully performed with only composed of both Ag_2S quantum dots and SnS_2 nanoplates.

Fig. 3 is the XPS analysis for 1% Ag_2S/SnS_2 composite. Fig. 3a reveals Sn, S and Ag elements are three main elements in Ag_2S/SnS_2 composites. Two obvious peaks at 487.0 and 495.3 eV could be attributed to the Sn $3d_{5/2}$ and Sn $3d_{3/2}$, respectively, in the Sn 3d high-resolution spectra (Fig. 3b).[44] Meanwhile, the typical peaks in Fig. 3c located at 161.7 and 162.9 eV could be assigned to S $2p_{3/2}$ and S $2p_{1/2}$ orbits of S^{2-}, respectively.[45] While the peaks at binding energy 368.3 and 374.5 eV could be ascribed to Ag $3d_{3/2}$ and Ag $3d_{5/2}$ of Ag^+ in Ag_2S quantum dots, respectively.[46] Above all, from the analysis of XRD, EDS and XPS, it can be confirmed that SnS_2 and Ag_2S exist in the Ag_2S/SnS_2 composites.

The light absorption abilities of pure SnS_2 and Ag_2S/SnS_2 composites were investigated *via* UV-vis spectroscopy. From Fig. 4a, we can see that SnS_2 has strong and broad absorption in the region of visible light, and Ag_2S quantum dot has broad absorption in both UV and visible light. Besides, the light absorption abilities of Ag_2S/SnS_2 composite materials show
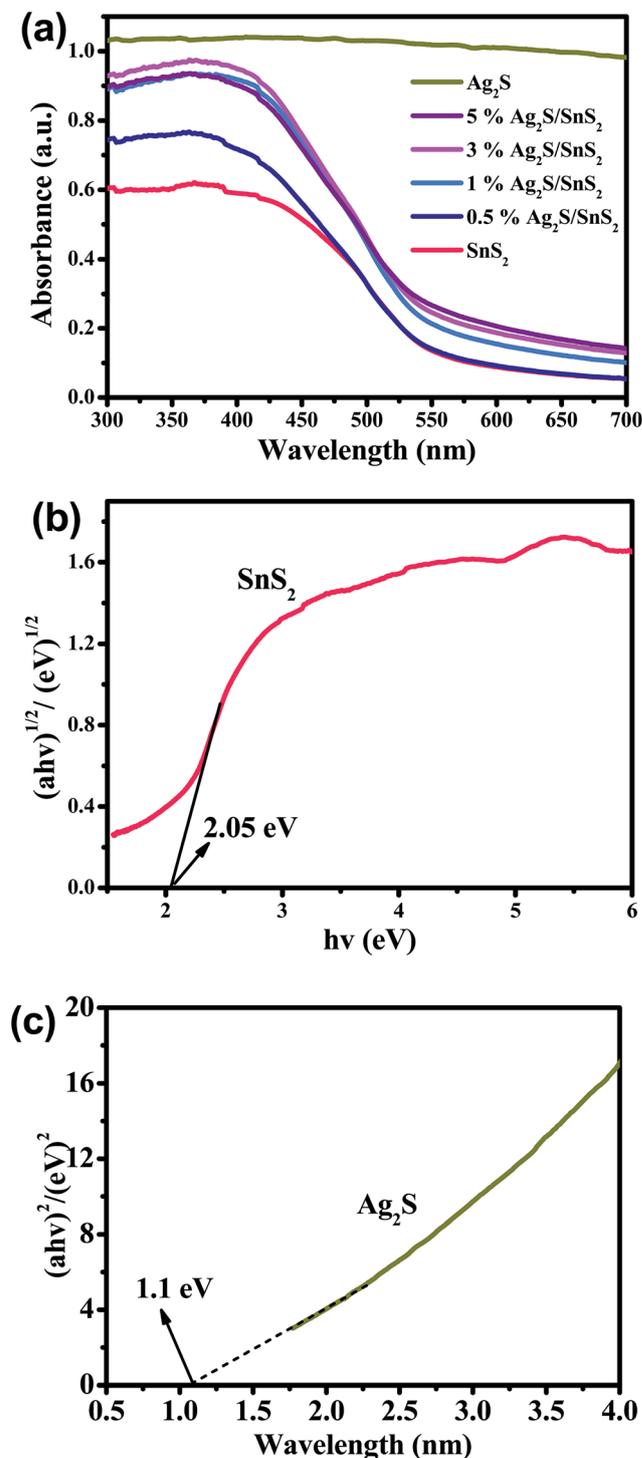

Fig. 4 (a) The optical absorption spectroscopy of SnS_2 and Ag_2S/SnS_2 composite materials; plots of $(ah\nu)^2$ and $(ah\nu)^{1/2}$ *versus* energy for the band gap energy of (b) SnS_2 and (c) Ag_2S, respectively.

enhancement with the addition of Ag_2S quantum dots. Hence the combination both SnS_2 and Ag_2S improves the absorption abilities, which may result in higher photocatalytic abilities for Ag_2S/SnS_2 composite materials. According to the equation: $ahv = A(hv - E_g)^{n/2}$, where a, h, v, A, E_g is absorption coefficient, Planck constant, light frequency, a constant and band gap energy, respectively.[47] The value of n is equal to 1 and 4 for direct and indirect transition semiconductors, respectively.[48] Thus, the values of n are 4 for SnS_2 and 1 for Ag_2S. The band gap energy of SnS_2 and Ag_2S were calculated to be 2.05 eV and 1.1 eV, respectively (as shown in Fig. 4b and c).

3.2 Photocatalytic activity

The photocatalytic properties of samples were evaluated by the degradation of MO (Fig. 5a) and the reduction of $Cr(VI)$ (Fig. 5b) under visible light irradiation. We can see from Fig. 5a, under visible light irradiation, MO is too stable to degrade without any photocatalysts, but about 68% MO is degraded with the addition of pure SnS_2. Meanwhile, in the case of Ag_2S/SnS_2 composite materials, MO degradation rates are enhanced for the same time period (60 min), and 1% Ag_2S/SnS_2 composite material shows the best photocatalytic activity with about 88% MO degraded. Besides, the removal rate of $Cr(VI)$ can quickly increase from 42% for pure SnS_2 to 53%, 57%, 51% and 45% for 0.5%, 1%, 3%, and 5% Ag_2S/SnS_2 composite materials, and the 1% Ag_2S/SnS_2 composite also shows the best performance, just

as shown in Fig. 5b. Above all, the *in situ* formation of Ag_2S makes good effect on the photocatalytic process.

The reaction kinetics of MO photocatalytic degradation over different samples were investigated by using a first-order kinetics model with the formula: $-\ln(C_t/C_0) = kt$. Where C_t and C_0 are the MO concentration at times t and 0, k (min^{-1}) is the rate constant of apparent first-order and t (min) is the irradiation time. According to the Fig. 5c, we can see the k for SnS_2, 0.5% Ag_2S/SnS_2, 1% Ag_2S/SnS_2, 3% Ag_2S/SnS_2 and 5% Ag_2S/SnS_2 are calculated to be 0.01822, 0.02787, 0.03228, 0.02352 and 0.02083 min^{-1}, respectively. The rate constant of 1% Ag_2S/SnS_2 composite is 1.77 times as high as the pure SnS_2 under the same conditions, indicating there has synergistic effect between Ag_2S and SnS_2, which improves the MO photocatalytic degradation. Moreover, the stability and recycling of the Ag_2S/SnS_2 materials were tested and shown in Fig. 5d, the photocatalytic performance has no significant decrease (only 3.2% decreased) after three cycles. The XRD and SEM analysis of 1% Ag_2S/SnS_2 composite after cycle runs were performed and the results are shown in Fig. S1 and S2.† For 1% Ag_2S/SnS_2 composite, the phase structure has no obvious changes before and after the experiment and the hexagonal structure still maintain with Ag_2S quantum dots intimately attached on the surface. The results confirm that the Ag_2S/SnS_2 has good stability.

Photoluminescence (PL) spectroscopy is usually used to investigate the transfer and recombination ability of photo-
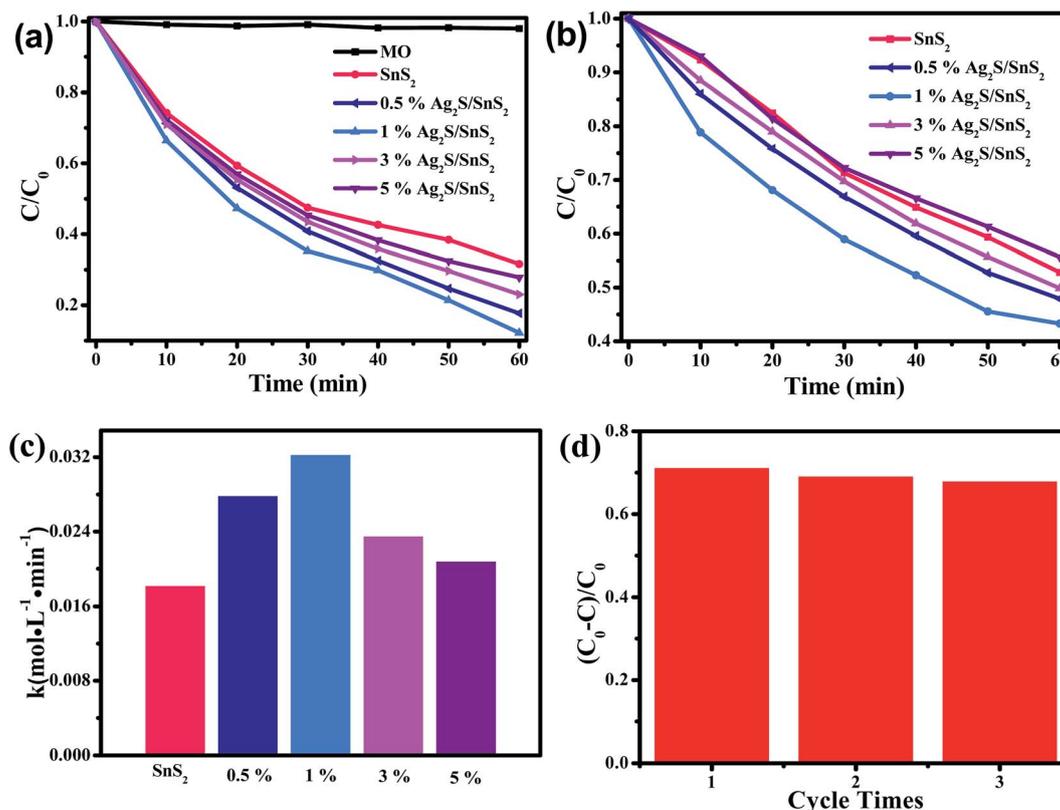

Fig. 5 The adsorption rate curves of MO (a) and Cr(VI) (b) test under visible light irradiation in the presence of as-prepared samples; (c) the corresponding rate constant (k) for photocatalytic degradation of MO solution over various samples under visible light irradiation; (d) cycling runs for the photodegradation MO in the presence of 1% Ag_2S/SnS_2 composites under visible light irradiation.

generated carriers in photocatalysts. Generally, the lower the PL emission intensity, the higher the efficiency of charge recombination, and the more charge can join in photocatalytic reaction, and finally, the higher the photocatalytic performance. The PL spectra of Fig. 6 show that the emission peaks positions of SnS_2 and 1% Ag_2S/SnS_2 are uniform, but the emission intensities of 1% Ag_2S/SnS_2 are lower than pure SnS_2, indicating Ag_2S/SnS_2 composite materials have lower recombination rate of carriers than pure SnS_2. The results show that the synergistic effect between Ag_2S and SnS_2 promotes the photo-induced carriers separation, and eventually, enhances the photocatalytic performance of Ag_2S/SnS_2 composite materials. EIS are performed on 1% Ag_2S/SnS_2 composite and pure SnS_2 to further determine the charge separation efficiency over different samples and the results are shown in Fig. 6b. We can see that the diameter of Ag_2S/SnS_2 composite is smaller than that of pure SnS_2, indicating the Ag_2S/SnS_2 composite has a relatively lower resistance than pure SnS_2. Therefore, the coupling of Ag_2S to SnS_2 can enhance the separation and transfer efficiency of charge, and realize enhanced photocatalytic performance.

It was generally accepted that holes (h^+), hydroxyl radical ($^•OH$), and superoxide radical ($^•O_2^-$) are three active species during photocatalytic oxidation processes.[49] The electron spin resonance (ESR) was executed with DMPO spin-trapping in methanol and water, respectively, to determine the major active species in the photocatalytic process, and the results are shown in Fig. 7. There is no ESR signal for Ag_2S/SnS_2 composites at dark condition, but the $DMPO^•O_2^-$ adducts signals can be observed under the visible light irradiation even the signal is not strong (Fig. 7a) and the $DMPO^•OH$ is still negligible (Fig. 7b), indicating that a handful of $^•O_2^-$ can be generated while $^•OH$ cannot be generated.[50] To further ascertain the active species over Ag_2S/SnS_2 photocatalyst, various active species trapping experiments were performed, just as shown in Fig. 8. After adding isopropanol (IPA) to trap $^•OH$, no obvious variation of photocatalytic efficiency can be observed, revealing the $^•OH$ was not the major active species.[51] However, the photocatalytic performance decreased in Ar atmosphere trapping $^•O_2^-$, and instantly decreased after the TEOA was added to trap the h^+.[52,53] Combining with ESR results, the $^•O_2^-$ have a littler effect on the

photodegradation process and the h^+ is the major active species in the photocatalysis reaction.

The value of valence band (VB) can be confirmed by the XPS analysis. Fig. 9 was the VB spectra of the pure SnS_2 sample and
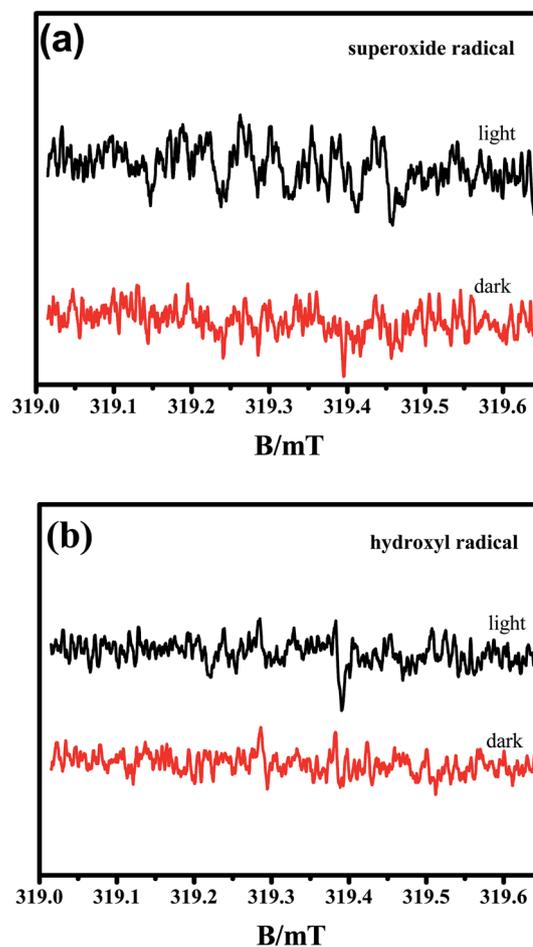
Fig. 7 ESR spectra of radical adducts trapped by DMPO in 1% Ag_2S/SnS_2 composite in (a) methanol dispersion (for $DMPO^•O_2^-$) and (b) aqueous dispersion (for $DMPO^•OH$) under visible light irradiation.
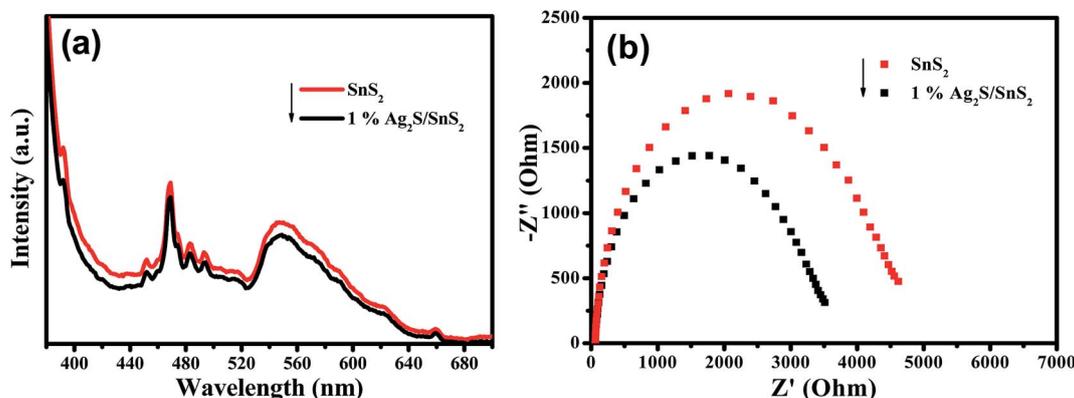
Fig. 6 (a) PL spectroscopy of SnS_2 and 1% Ag_2S/SnS_2 composite; (b) electrochemical impedance spectroscopy plots of 1% Ag_2S/SnS_2 composite and pure SnS_2.
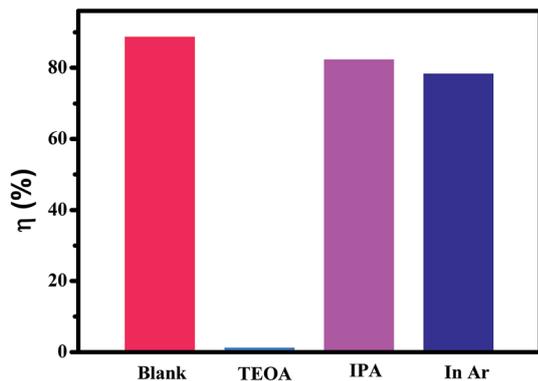
Fig. 8 Effects of various scavengers on the visible light photocatalytic activity of the 1% Ag_2S/SnS_2 composite material.

Fig. 10 The possible reaction mechanism for photocatalytic process with Ag_2S/SnS_2 composite material.

the VB maximum edge can be estimated to be 1.30 eV. According to the DRS results, the band gap energy (E_g) of pure SnS_2 is 2.05 eV. Based on the equations $E_{VB} = E_{CB} + E_g$, the CB potential of SnS_2 can be calculated to be −0.75 eV. Fig. 10 illustrates the possible mechanisms for the increased photocatalytic activity of Ag_2S/SnS_2 sample towards the pollutant degradation. After the visible light irradiated on the Ag_2S/SnS_2 composites, the electrons in the VB of SnS_2 and Ag_2S could be inspired and transfer from VB to the CB and the photo-generated holes would leaving in the VB. Generally, most of electrons and holes would recombine rapidly for pure SnS_2, which results in pure SnS_2 having relatively poor photocatalytic activity. However, when Ag_2S quantum dots was *in situ* formed on the surface of the SnS_2, the most electrons would transfer from the CB of SnS_2 to the more positive CB of Ag_2S due to the excellent electron transfer ability of Ag_2S, leading to effective separation of charge carriers.[54–56] But there still have a handful of electrons don't transferred, which would reduce the adsorbed molecule oxygen to yield $^{\bullet}O_2^-$, and because the remaining electrons are little, the content of $^{\bullet}O_2^-$ is few. Then the produced few $^{\bullet}O_2^-$ and vast photo-generated holes would worked as the reactive oxygen species for the subsequently photocatalytic degradation reaction. The excellent
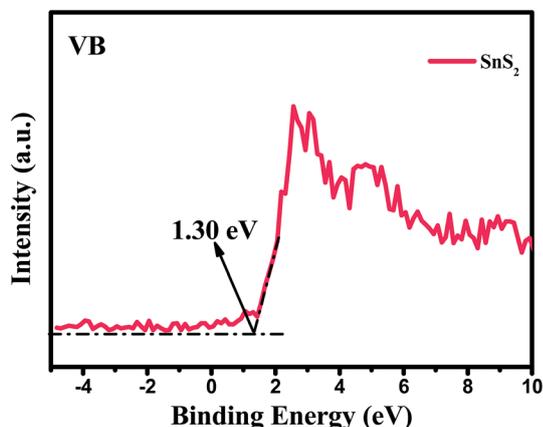
photocatalytic performance of Ag_2S/SnS_2 composite photo-catalyst material can be attributed to the positive effect of Ag_2S quantum dots, which provides an effective way to prevent the recombination of photo-generated carriers.

4. Conclusions

In summary, high efficient Ag_2S/SnS_2 composite photocatalysts were successfully fabricated *via* a facile *in situ* hydrothermal-ion-exchange method. The photocatalytic ability of Ag_2S/SnS_2 composite materials toward MO and Cr(VI) under visible light irradiation is considerably enhanced compared to pure SnS_2. The introduction of Ag_2S quantum dots in the composites resulted in enhanced and stability photocatalytic performance, which provides an effective way for the separation of photo-generated carriers. The major active species were determined to be holes (h^+) and superoxide radical ($^{\bullet}O_2^-$) in photocatalytic reaction. Moreover, this work provided meaningful information on the preparation of other metal sulfide composite materials.

Conflicts of interest

There are no conflicts to declare.

Acknowledgements

References

1 Z. Yu, B. S. Yin, F. Y. Qu and X. Wu, *Chem. Eng. J.*, 2014, **258**, 203–209.

Fig. 9 Valence-band XPS spectra of pure SnS_2.

2   S. C. Xu, S. S. Pan, Y. Xu, Y. Y. Luo, Y. X. Zhang and G. H. Li, *J. Hazard. Mater.*, 2015, **283**, 7–13.

3   Z. Pei, M. Zhu, Y. Huang, Y. Huang, Q. Xue, H. Geng and C. Zhi, *Nano Energy*, 2016, **20**, 254–263.

4   S. Ma, J. Xie, J. Wen, K. He, X. Li, W. Liu and X. Zhang, *Appl. Surf. Sci.*, 2017, **391**, 580–591.

5   K. Nakata and A. Fujishima, *J. Photochem. Photobiol., C*, 2012, **13**, 169–189.

6   M. Barroso, A. J. Cowan, S. R. Pendlebury, M. Grätzel, D. R. Klug and J. R. Durrant, *J. Am. Chem. Soc.*, 2011, **133**, 14868–14871.

7   S. W. Zhang, J. X. Li, X. K. Wang, Y. S. Huang, M. Y. Zeng and J. Z. Xu, *J. Mater. Chem. A*, 2015, **3**, 10119–10126.

8   W. M. Wu, G. D. Liu, Q. H. Xie, S. J. Liang, H. R. Zheng, R. S. Yuan, W. Y. Su and L. Wu, *Green Chem.*, 2012, **14**, 1705–1709.

9   Y. J. Yuan, Z. J. Ye, H. W. Lu, B. Hu, Y. H. Li, D. Q. Chen, J. S. Zhong, Z. T. Yu and Z. G. Zou, *ACS Catal.*, 2016, **6**, 532–541.

10 L. C. A. Oliveira, H. S. Oliveira, G. Mayrink, H. S. Mansur, A. A. P. Mansur and R. L. Moreir, *Appl. Catal., B*, 2014, **152–153**, 403–412.

11 X. Q. An, J. C. Yu and J. W. Tang, *J. Mater. Chem. A*, 2013, **2**, 1000–1005.

12 Y. D. Zhang, P. Y. Zhu, L. L. Huang, J. Xie, S. C. Zhang, G. S. Cao and X. B. Zhao, *Adv. Funct. Mater.*, 2015, **25**, 481–489.

13 O. Brontvein, A. Albu-Yaron, M. Levy, D. Feuerman, R. Popovitz-Biro, R. T. A. Enyashin and J. M. Gordon, *ACS Nano*, 2015, **9**, 7831–7839.

14 C. Wang, L. Wang, J. Jin, J. Liu, Y. Li, M. Wu, L. H. Chen, B. J. Wang, X. Y. Yang and B. L. Su, *Appl. Catal., B*, 2016, **188**, 351–359.

15 S. Liang, Z. Zhou, X. Wu, S. Zhu, J. Bi, L. Zhou, M. Liu and L. Wu, *Molecules*, 2016, **21**, 213–226.

16 F. W. Li, L. Chen, M. Q. Xue, T. Williams, Y. Zhang, D. R. MacFarlane and J. Zhang, *Nano Energy*, 2017, **31**, 270–277.

17 X. Zhang, P. Zhang, L. J. Wang, H. Q. Gao, J. T. Zhao, C. H. Liang, J. H. Hu and G. S. Shao, *Appl. Catal., B*, 2016, **192**, 17–25.

18 F. Deng, L. N. Zhao, X. L. Pei, X. B. Luo and S. L. Luo, *Mater. Chem. Phys.*, 2017, **189**, 169–175.

19 G. W. Li, R. Su, J. C. Rao, J. Q. Wu, P. Rudolf, G. R. Blake, R. A. de Groot, F. Besenbacher and T. T. M. Palstra, *J. Mater. Chem. A*, 2016, **4**, 209–216.

20 M. He, L. X. Yuan and Y. H. Huang, *RSC Adv.*, 2013, **3**, 3374–3383.

21 A. Yella, E. Mugnaioli, M. Panthöfer, H. A. Therese, U. Kolb and W. Tremel, *Angew. Chem., Int. Ed.*, 2009, **48**, 6426–6430.

22 P. Wu, N. Du, H. Zhang, J. Liu, L. Chang, L. Wang, D. Yang and J. Z. Jiang, *Nanoscale*, 2012, **4**, 4002–4006.

23 C. X. Zhai, N. Du, H. Zhang and D. Yang, *Chem. Commun.*, 2011, **47**, 1270–1272.

24 F. Deng, X. Y. Lu, X. L. Pei, X. B. Luo, S. L. Luo and D. D. Dionysiou, *J. Hazard. Mater.*, 2017, **332**, 149–161.

25 J. F. Qu, D. Y. Chen, N. J. Li, Q. F. Xu, H. Li, J. H. He and J. M. Lu, *Appl. Catal., B*, 2017, **207**, 404–411.

26 J. L. Mu, H. Miao, E. Z. Liu, L. D. Chen, J. Feng, T. X. Han, Y. Gao, J. Fan and X. Y. Hua, *Ceram. Int.*, 2017, **43**, 4992–5001.

27 H. Liu, D. Lu, Z. Zhang, G. Jie, Y. Yang and Z. Zhu, *J. Mater. Sci.*, 2015, **50**, 3207–3211.

28 X. Li, J. Zhu and H. Li, *Appl. Catal., B*, 2012, **123–124**, 174–181.

29 S. Y. Hong, R. Popovitz-Biro, Y. Prior and R. Tenne, *J. Am. Chem. Soc.*, 2003, **125**, 10470.

30 Z. Yang, X. Huang, J. Li, Y. Zhang, S. Yu, Q. Xu and X. Y. Hu, *Mikrochim. Acta*, 2012, **177**, 381–387.

31 F. Deng, X. Y. Lu, X. L. Pei, X. B. Luo, S. L. Luo and D. D. Dionysiou, *J. Hazard. Mater.*, 2017, **332**, 149–161.

32 Z. Zhang, J. Huang, M. Zhang, Q. Yuan and B. Dong, *Appl. Catal., B*, 2015, **163**, 298–305.

33 H. Liu, L. Deng, Z. F. Zhang, J. Guan, Y. Ying and Z. F. Zhu, *J. Mater. Sci.*, 2015, **50**, 3207–3211.

34 Y. Xie, S. H. Heo, Y. N. Kim, S. H. Yoo and S. O. Cho, *Nanotechnology*, 2010, **21**, 015703.

35 H. M. Jia, W. W. He, W. G. Wamer, X. N. Han, B. B. Zhang, S. Zhang, Z. Zheng, Y. Xiang and J. J. Yin, *J. Phys. Chem. C*, 2016, **118**, 21447–21456.

36 K. Ikeue, Y. Shinmura and M. Machida, *Appl. Catal., B*, 2012, **123–124**, 84–88.

37 B. Subash, B. Krishnakumar, M. Swaminathan and M. Shanthi, *Spectrochim. Acta, Part A*, 2013, **105**, 314–319.

38 D. A. Reddy, R. Ma, M. Y. Choi and T. K. Kim, *Appl. Surf. Sci.*, 2015, **324**, 725–735.

39 X. Yang, H. T. Xue, J. Xu, X. Huang, J. Zhang, Y. B. Tang, T. W. Ng, H. L. Kwong, X. M. Meng and C. S. Lee, *ACS Appl. Mater. Interfaces*, 2014, **6**, 9078–9084.

40 Y. Xie, S. H. Heo, Y. N. Kim, S. H. Yoo and S. O. Cho, *Nanotechnology*, 2010, **21**, 015703.

41 B. Zeng and W. Zeng, *Nano*, 2016, **12**, 1750005.

42 L. Y. Mao, J. J. Li, Y. L. Xie, Y. J. Zhong and Y. Hu, *RSC Adv.*, 2014, **4**, 29698–29701.

43 X. L. Hu, Y. Y. Li, J. Tian, H. R. Yang and H. Z. Cui, *J. Ind. Eng. Chem.*, 2017, **45**, 189–196.

44 L. L. Chen, M. Chen, D. L. Jiang and J. M. Xie, *J. Mol. Catal. A: Chem.*, 2016, **425**, 174–182.

45 D. Jiang, L. Chen, J. Xie and M. Chen, *Dalton Trans.*, 2014, **43**, 4878–4885.

46 H. L. Zhang, B. Wei, L. Zhu, J. H. Yu, W. J. Sun and L. L. Xu, *Appl. Surf. Sci.*, 2013, **270**, 133–138.

47 M. Y. Xu, H. L. Niu, J. J. Huang, J. M. Song, C. J. Mao, S. Y. Zhang, C. F. Zhu and C. L. Chen, *Appl. Surf. Sci.*, 2015, **351**, 374–381.

48 J. Tian, T. J. Yan, Z. Qiao, L. L. Wang, W. J. Li, J. M. You and B. B. Huang, *Appl. Catal., B*, 2017, **209**, 566–578.

49 Y. F. Liu, W. Q. Yao, L. Di, R. L. Zong, M. Zhang, X. G. Ma and Y. F. Zhu, *Appl. Catal., B*, 2015, **163**, 547–553.

50 Z. Ma, J. Yu and S. Dai, *Adv. Mater.*, 2010, **22**, 261–285.

51 R. Qiao, M. M. Mao, E. L. Hu, Y. J. Zhong, J. Q. Ning and Y. Hu, *Inorg. Chem.*, 2015, **54**, 9033–9039.

52 A. Etogo, E. L. Hu, C. M. Zhou, Y. J. Zhong, Y. Hu and Z. L. Hong, *J. Mater. Chem. A*, 2015, **3**, 22413–22420.

53 X. H. Gao, H. B. Wu, L. X. Zheng, Y. J. Zhong, Y. Hu and X. W. Lou, *Angew. Chem.*, 2014, **126**, 6027–6031.

54 H. L. Zhang, B. Wei, L. Zhu, J. H. Yu, W. J. Sun and L. L. Xu, *Appl. Surf. Sci.*, 2013, **270**, 133–138.

55 D. Jiang, L. Chen, J. Xie and M. Chen, *Dalton Trans.*, 2014, **43**, 4878–4885.

56 Y. Wang, M. X. Sun, Y. L. Fang, S. F. Sun and J. He, *J. Mater. Sci.*, 2016, **51**, 779–787.